arXiv:1304.1444v1 [physics.space-ph] 4 Apr 2013

Reconnection and electron temperature anisotropy in electron scale plasma turbulence

Christopher T. Haynes,[1, a)] David Burgess,[1] and Enrico Camporeale[2]
[1)]School of Physics and Astronomy, Queen Mary University of London, Mile End Road, London E1 4NS, UK
[2)]T-5 Applied Mathematics and Plasma Physics, Los Alamos National Laboratory, Los Alamos, NM 87545, USA

We study the turbulent decay of fluctuations using results from two dimensional, particle-in-cell (PIC) collisionless plasma simulations with realistic electron-proton mass ratio and a guide field out of the simulation plane. A fluctuation power spectrum with approximately power law form is created down to scales of order the electron gyroradius. Where there is an X-point magnetic field line geometry we find signatures of reconnection such as electron bulk inflows and outflows. The reconnection signatures persist even at small scales even when the reconnection sites are only several electron gyroradii across. Although the reconnection sites do not dominate the electron temperature variation, they are generally associated with regions of strong parallel electron temperature anisotropy. By tracking simulation particles we find that electrons are accelerated along the guide field near reconnection sites, and that in the reconnection outflows there is a mixing of electrons from spatially separated locations. The topology of magnetic field lines connected to the reconnection site allows this mixing of different electron populations, and the formation of multi-peaked velocity distribution functions, and consequently strong parallel temperature anisotropy. In a fully three-dimensional system the multi-peaked distribution functions would be expected to generate further waves via kinetic instabilities. The proposed mechanism of generating anisotropy within collisionless plasma turbulence will be relevant to space and astrophysical systems, where there is evidence that the evolution of the plasma is associated with temperature anisotropy instability thresholds. The presence of reconnection sites leads to electron energy gain, nonlocal velocity space mixing and the formation of strong temperature anisotropy; this is evidence of an important, but not yet quantified, role for reconnection in the dissipation of turbulent fluctuations.

I. INTRODUCTION

Turbulence in solar system plasmas is studied as an example of a universal dissipation process which is important across a gamut of astrophysical systems. Solar wind fluctuations are an example of turbulence[1] in a magnetized, low collisionality and expanding plasma with characteristic properties such as anisotropy[2,3] and distribution functions constrained by kinetic plasma instabilities.[4] Turbulence in astrophysical plasmas, as in hydrodynamics, acts to transfer energy from large to small scales. The energy distribution of hydrodynamic homogeneous turbulence follows a universal power law, or Kolmogorov spectrum with energy scaling as $k^{-5/3}$. Observational data from the Cluster mission[5] shows that the same is true in the solar wind plasma at large scales for $k\lambda_i \ll 1$, where λ_i is the ion inertial length. Observational data is less well explained at electron scales, but the existing data shows that the power law steepens at smaller scales[6]. Simulations suggest the inclusion of plasma wave modes, such as kinetic Alfvén waves (KAW)[7] adds additional damping to the ions and/or electrons, resulting in the change in power law. The exact form of the power law steepening is still unclear, but one line of thinking is that at some "break point" in wavenumber some extra dissipation mechanism(s) associated with kinetic scales or plasma compression begins to act, and a different power law applies after that point.[5] An alternative suggestion is that after the initial break point in wavenumber some form of exponential fit, rather than a single power law, applies for higher wavenumber.[8]

Magnetic reconnection, another universal plasma process, changes the magnetic field line topology and mediates energy release from the magnetic field. It is seen at boundaries such as the magnetopause[9] and in the solar wind[10], and it is recognized as a fundamental process in laboratory[11] and astrophysical plasmas[12]. It is clear that the processes of magnetic reconnection and energy cascade to short scales could act together in a turbulent plasma, especially if the magnetic field is heavily perturbed by the turbulent motion of the plasma. Servidio et al.[13] have made the case that reconnection should be viewed as an important process within plasma turbulence: "it would be difficult to envision a turbulent cascade that proceeds without change of magnetic topology." In a turbulent cascade, energy (both magnetic and kinetic) is transported from large to small scales. The conventional picture is that at some small scale length the cascade is terminated by some dissipation, or plasma heating process, which damps the turbulent fluctuations. On the other hand, magnetic reconnection acts to convert magnetic energy to thermal and kinetic plasma energy and in doing so acts to relax the complexity in the magnetic field topology. Thus if the turbulent cascade also transports magnetic field topological complexity to small scales, the question arises as to what mechanisms govern plasma turbulence in the presence of reconnection, and on what scales do they operate.

Observations of reconnection within turbulence, away from boundaries such as the magnetopause, are rare. Some evidence has been presented of reconnection events associated with magnetic nulls in the large amplitude turbulence in the solar wind, downstream of the quasi-parallel part of the

---

[a)]Electronic mail: c.t.haynes@qmul.ac.uk

Earth's bow shock[14]. The observations were interpreted in the context of thin current sheets between magnetic islands, and a reconnection geometry with Hall currents (Fig. 1, Ref. 14). There have been other observations offering indirect evidence of reconnection contributing to solar wind dissipation[15,16].

Turbulence is inherently multi-scale: the forcing and inertial range are at scales where a fluid-like model, such as MHD, would seem to be appropriate, and the larger of those scales are generally well separated from the kinetic scales at which dissipation via cyclotron or Landau processes is expected to operate. Even in the kinetic regime there is a further separation of scales between ion and electrons. The vast range of scale required for a full description poses fundamental problems for simulations, and, in general, different simulation models are used to study different, restricted ranges of scale. MHD simulations of reconnection have tended to concentrate on simplified geometries and boundary conditions more suited to boundaries between topologically distinct regions. However, a general characteristic found in MHD simulations of turbulence is the formation of thin current sheets, which are expected to be possible sites for reconnection. The statistical properties of reconnection sites in two-dimensional MHD turbulence have recently been investigated, suggesting that strong reconnection events can occur locally in turbulence.[17] The use of particle (full particle or hybrid) simulations enables the study of kinetic processes that might lead to dissipation of turbulent fluctuations. Usually some form of simplification has to be assumed to make such simulations tractable, either by restricting the spatial domain, or using unrealistic electron-proton mass ratios. An additional problem is the noise floor imposed by using a finite number of particles, which reduces the dynamic range of any turbulent cascade. The choice of a small number of simulation particles might mean that behavior leading to a turbulent cascade is masked, or truncated in wavenumber. Implicit PIC simulations with realistic mass ratio, albeit with a restricted spatial domain, have shown the development of power law behavior and power anisotropy even down to electron scales.[18]. Ref. 18 also contains a comparison of different simulations in terms of scale sizes, mass ratios and noise floor. With sufficient computational resource it is possible to simulate aspects of kinetic coupling across ion to electron scales,[19] albeit with unrealistic mass ratio.

Recent simulation work using kinetic models on the dissipation regime has emphasized the roles of wave modes such as kinetic Alfvén waves (KAW)[20] or whistler mode turbulence.[21] Although solar wind observations appear to favor the presence of KAW,[22] other simulations have shown more ambiguous signatures.[18] Hybrid simulations performed by Perrone and Valentini[23] show that the response of the ion species (which can include alpha particles) to be anisotropic heating that favors the perpendicular direction, whilst suggesting the presence of whistler and KAWs. On the other hand, very large scale simulations[19] point to the formation of coherent structures, and anisotropic electron current heating in current sheets, and also the formation of fast magnetosonic modes being launched into the plasma by the large scale movement of the larger vortex and island structures. It is not unreasonable to expect dissipation in the kinetic regime to be a combination of non-linear processes, and the damping of linear wave modes transferring energy to particle kinetic energy. The relative importance of such processes is still an open field of study.

In this paper, we aim to supplement recent works by presenting results of fully kinetic plasma simulations with a realistic mass ratio and plasma parameters (such as the ratio of plasma frequency to gyrofrequency) which are relevant to the solar wind. The high mobility of electrons to that of ions (at the same temperature) will have important physical effects, not necessarily probed by other simulations. This paper will therefore focus on processes at electron scales, and will concentrate on electron flows and velocity distributions. We aim to show the relationship between reconnection and turbulence in this regime, and in particular to show that reconnection can be responsible for strong electron temperature anisotropy within turbulence. We also find that reconnection sites within turbulence can be considered as plasma mixing zones, generating multi-peaked distributions in electron velocity space, which could be a source of further waves and particle coupling via instabilities.

Kinetic simulations of collisionless plasmas, whether PIC, hybrid or Vlasov, produce approximate solutions of the Vlasov-Maxwell system. Thus it is worthwhile considering what is meant by dissipation in these models in the context of turbulence. In hydrodynamic, or collisional plasma turbulence the link between wave damping and dissipation is relatively clear since collisionality provides an irreversible process. In a collisionless system it is tempting to concentrate on particle heating, calculated from the kinetic temperature, and consider that as a measure of dissipation. For example, wave damping, whether Landau or cyclotron, and the consequent increase in particle kinetic temperature, is usually invoked as a dissipation mechanism. However, in a system which is locally inhomogeneous, with regions of different field line topology (as in turbulence in a magnetized plasma) the issue of identifying dissipation, or finding a suitable measure of dissipation is more difficult. For example, the collisionless Vlasov equation preserves entropy, so Landau damping cannot be regarded as a simple process of thermalization, i.e., turning ordered information into heat. On the other hand, it is possible that, for a turbulent system far from equilibrium, some form of generalized entropy[24] is more appropriate for evaluating dissipation. And, bearing in mind the fact that PIC simulations are only approximate solutions of the Vlasov system, it is likely that they have some form of effective pseudo-collisionality, e.g., due to finite particle number. Thus it might be possible that irreversibility is introduced by the simulation method itself. These rather fundamental questions will not be addressed in this paper, but our simulation results do indicate that the presence of reconnection sites leads to electron energy gain, non-local velocity space mixing and the formation of strong temperature anisotropy. We suggest that this is evidence of an important, but not yet properly quantified, role for reconnection in the dissipation of turbulent fluctuations at electron scales.

II. METHODOLOGY

We use the particle-in-cell (PIC) code Parsek2D,[25] which is based on the implicit moment method for time advance of the electromagnetic fields, and a predictor-corrector method for the particle mover. The implicit method allows larger time steps and box sizes compared with explicit PIC methods, which are usually constrained (for numerical stability) by the condition $\omega_{pe}\Delta t < 2$, where Δt is the time step, and ω_{pe} is the electron plasma frequency. Also Parsek2D allows a relaxation of the Courant-Friedrichs-Lewy (CFL) condition $c\Delta t/\Delta x < 1$, where c is the speed of light and Δx is the cell size. We choose a time step $\Delta t = 0.05\Omega_e^{-1}$, where Ω_e is the electron gyrofrequency. The code allows cell sizes larger than a Debye length λ_D, and in these simulations $\Delta x = \Delta y \sim 17\lambda_D$. The code is two dimensional in the x-y plane but retains all three vector components for velocities and fields. The electron-proton plasma is initially loaded with a uniform, isotropic Maxwellian distribution. The simulation box is 200×200 cells, with periodic boundary conditions and 6400 simulation particles per cell for each species. This large number of particles reduces the statistical particle noise so that the dynamic range in Fourier space is large enough to resolve the formation of a turbulent cascade. The simulation box is sized to resolve wave vectors ranging from $k\rho_e = 0.1$ to $k\rho_e = 10$, where k is wave vector and ρ_e the thermal electron gyroradius. The box length is about 1 ion inertial length, and the electron gyro-motion is resolved with ~ 2 cells per electron gyroradius (based on the initial guide field strength). We choose plasma parameters which are appropriate to the solar wind. The ratio of ion plasma frequency to ion cyclotron frequency ω_{pi}/Ω_i is about 1650, and the ion to electron mass ratio is physical with $m_i/m_e = 1836$. The ions and electrons are initialized at the same temperature $\beta_e = \beta_i = 0.5$. The simulation was run for a period of $T = 200\Omega_e^{-1}$.

We initialize the simulation with a magnetic guide field $\mathbf{B}_0$ in the out of plane direction z, and add random long wavelength magnetic field fluctuations as in earlier simulations, using the same parameters as Camporeale et al.[18] The intention is to provide an initial input of energy at low values of k with properties mimicking a turbulent field and then follow the decay of this initial perturbation and the development of power at larger wave numbers. The magnetic field is initialized with random fluctuations in all three components for wave vectors $k_x = 2\pi m/L_x$ and $k_y = 2\pi n/L_y$ for $m = -3, \ldots, 3$ and $n = -3, \ldots, 3$. We do not impose any spectral slope on the initial fluctuations. The initial electric field is zero, but the abrupt perturbation of the magnetic field acts to initialize the self-consistent evolution of the turbulent decay after a short period at the start of the simulation. This method emphasizes the random nature of turbulence, and in particular has the advantage that no particular linear modes are assumed dominant. Other methods of initializing the decay of turbulent fluctuations are possible including using initial equilibria[19], alfvénic-like fluctuations[18], or superpositions of linear modes.[21]

If the initial fluctuations at small k have large enough amplitude there will be regions favorable for strong reconnection. The requirement to resolve the development of a turbulent cascade also means that relatively large values have to be used for the initial perturbations. This implies there will be strong non-linearities at small values of k. The upper limit of the field perturbation was set to $\delta B/B_0 = 1$, where B_0 is the amplitude of the background guide magnetic field. The choice of a configuration with the average guide field perpendicular to the simulation plane does not support $k_\parallel$ wave vectors (at least on average), but does favor magnetic field line topologies with islands and X-points with a guide field.

We identify magnetic field X-points as potential reconnection sites using the technique described by Servidio et al.[17]. The vector potential A_z is computed from the magnetic field; contours of constant A_z represent magnetic field lines in the x-y simulation plane. For each cell we calculate the Hessian matrix for A_z and its eigenvalues. If the eigenvalues are of opposite sign, then the location is a saddle point, and if the gradient of A_z is also zero then this is a potential location for reconnection. Since the simulation is discrete in space a threshold is used to indicate a possible zero gradient. This method may find multiple locations around a single reconnection point, and in this case the cell with the lowest gradient of A_z is taken to be the actual center. Additionally we use in-plane field lines to confirm the calculated positions of reconnection sites, and in order to compare the field line geometry and motion with the electron bulk velocities.

III. RESULTS

Figure 1 shows the initial and final magnetic field line configurations for the simulation at times $T = 0$ and $T = 200\Omega_e^{-1}$. Potential X-point reconnection sites are shown by black crosses where the threshold for the gradient is satisfied. Sometimes a single X-point will be shown as a cluster of cells satisfying the magnetic geometrical criterion. The end state has a magnetic field which is topologically simpler with 8 X-point sites compared to 10 initially, although of those 8 several seem on the point of disappearing. This behavior is also seen in the reduction of the number of magnetic islands. During the simulation the field line evolution is highly dynamic, with X-points moving around the simulation region and interacting with magnetic islands and other X-points. Animations show that magnetic islands gain or lose flux via reconnecting field line motion through X-points, i.e., field lines with island-like connectivity become linked to other X-points or encircle more than one island. Thus an island may shrink until it disappears or is absorbed by another island, and at this point the separating X-point also disappears. We also see that the sense of reconnection may reverse at an X-point, with the movement of field lines changing direction as the surrounding islands evolve. The effect is that any particular island may be growing or shrinking at different times in the simulation. In the final state there are some X-points which are in complex geometries and seem on the verge of disappearing if the simulation were run longer. By examining the time evolution of the local electron gyroradius we find that once an X-point region develops a scale less than about an electron gyrodiameter it is likely that the X-point will disappear, although sometimes

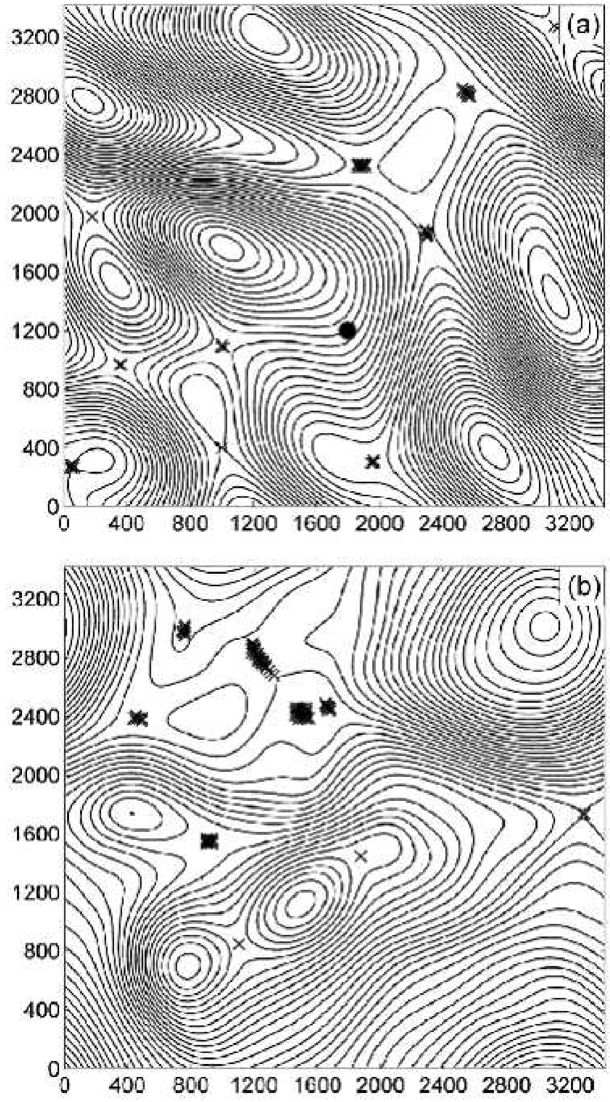

FIG. 1. Initial and final magnetic field line configurations at (a) T=0 and (b) $T = 200\Omega_e^{-1}$. Lengths in units of λ_D.

disappearance occurs in more topologically complex regions with several X-points close to each other.

Figure 2 shows the power spectra of $|\delta B|^2/|B_0|^2$ as a functions of k_x and k_y for the simulation at $T = 0$ (green) and $T = 100\Omega_e^{-1}$ (blue). The noise floor of the simulation (determined from a simulation with no perturbation applied) is shown in red. The k_x and k_y directions are both perpendicular to the average guide field and show essentially the same behavior. Starting from the initial energy input at small k values, the power at larger k evolves rapidly until a relatively time steady spectrum develops. There are no major differences between the spectra in the two directions. Earlier work with the guide field in the simulation plane showed similar rapid formation of approximately power law spectra, but also anisotropy in the parallel and perpendicular wave vector power spectra.[18] The simulation scale size is approximately one ion inertial length λ_i, and between this and $k\rho_e = 1$ the power spectrum is approximately proportional to $k^{-8/3}$ in agreement with other simulations and observational data.[5,26] Beyond this scale, the spectra steepen, consistent with observations, but there appears to be no obvious break point in wavenumber, and instead the gradient gradually increases with increasing values of k. Note that for $k\rho_e \geq 4$ the spectrum is not above the background noise level and is not meaningful. The behavior of the spectra apparently confirm the formation of a turbulent cascade down to the noise level of the simulation and scales of order the electron gyroradius.

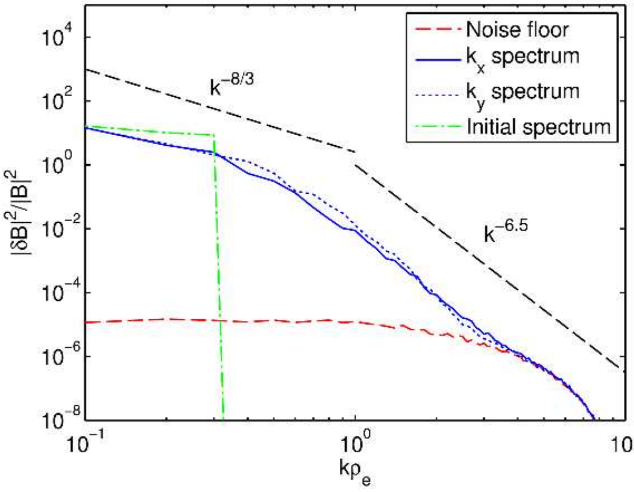

FIG. 2. Power spectra of $|\delta B|^2/|B_0|^2$ as functions of k_x and k_y, at $T = 100\Omega_e^{-1}$.

A. Electron Drift and Temperature Anisotropy

Reconnection is usually understood to produce plasma heating, and so, naively, one might expect to find increased electron temperature around magnetic field X-points. However, neither electron nor ion temperature is seen to significantly increase in the vicinity of the identified reconnection sites when compared to variations seen in other locations over the course of the simulation. This possibly indicates that any energy dissipation that occurs through the reconnection process does not dominate over dissipation not associated with reconnection sites. But heating in itself is not a definitive proxy for dissipation, since the heating process might be wholly or partly reversible. Furthermore, at reconnection sites one has to account for the fact that magnetic energy has also been converted into other forms of kinetic energy, such as electron bulk velocity, rather than just heating the ions/electrons. Consequently, in order to illustrate the effects of reconnection around magnetic field X-points, we concentrate on the electron drift velocity and temperature anisotropy.

Figure 3 shows the full simulation domain at time $T = 97\Omega_e^{-1}$, with the electron temperature anisotropy $(T_{e\parallel}/T_{e\perp})$, and magnetic field lines shown in black. Although electron temperature does not significantly increase at reconnec-

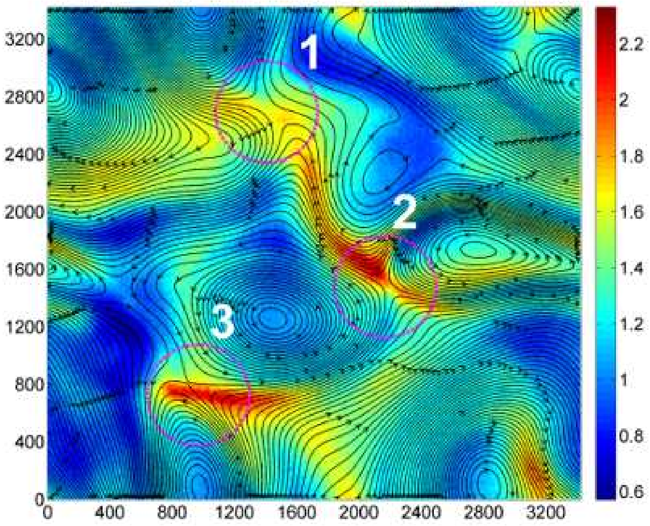

FIG. 3. Magnetic field lines (black) and electron temperature anisotropy $(T_{e\parallel}/T_{e\perp})$ at time $T = 97\Omega_e^{-1}$ for the full simulation domain. The three X-point regions discussed in the text are marked.

tion sites, this plot shows that electron parallel temperature anisotropy is enhanced at certain sites. Three reconnection sites have been labeled as showing strong parallel temperature anisotropy, although not all such sites in the figure show this feature as clearly. Our analysis will focus on these three sites in order to understand how this particular signature arises, and how it is associated with magnetic reconnection.

Figure 4(a) shows an enlarged detail for reconnection site 2, and Fig. 4(b) shows similar for reconnection site 3. Bulk electron drifts are shown in white and magnetic field lines in black. The geometry of the magnetic field lines and electron flows in Fig.4(a) resemble a typical X-point reconnection configuration with inflow and outflow regions. However, the centers of the velocity and the magnetic field patterns are displaced by ~ 50 debye lengths due to the lack of symmetry of the surrounding magnetic islands. This fluid-like configuration is perhaps surprising at this scale, given that the size of the reconnection site ~ 400 debye lengths (25 cells) compared to the electron thermal gyroradius of ~ 80 debye lengths (5 cells). This electron flow signature is not unusual, and appears at the other sites, as demonstrated by Fig. 4(b) for reconnection site 3, where the centers of the flow and field patterns are displaced by $\sim 100\lambda_D$. This is even more than at reconnection site 2, due to the larger asymmetry imposed by the surrounding islands.

Reconnection sites 2 and 3 are both at the junction of merging magnetic islands. Reconnection site 1 is located in a complex magnetic topology, and its sense of field line motion changes as the local islands around it disappear. Despite this, the site does show a large electron parallel temperature anisotropy and an electron flow signature similar to those of the other two reconnection sites.

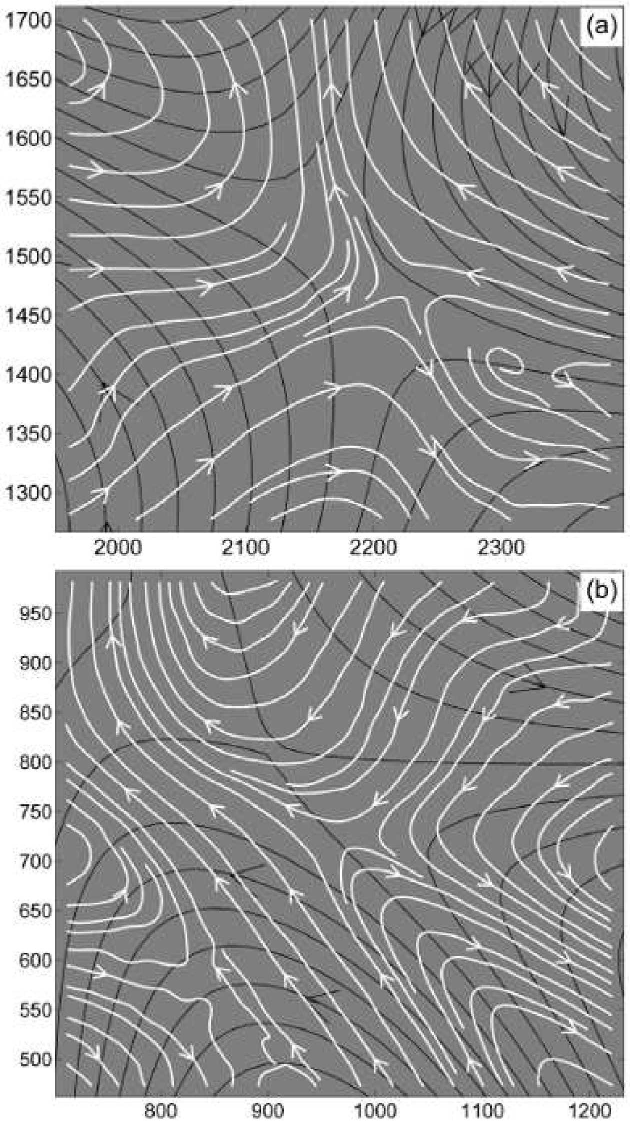

FIG. 4. Enlarged detail showing magnetic field lines (black) and electron bulk drifts (white) for (a) reconnection site 2, and (b) reconnection site 3. The position of the reconnection sites are marked in Fig. 3.

Figure 5 shows another feature of magnetic reconnection at electron scales that can be identified in the locality of the X-points. Reconnection site 2 is shown, with field lines plotted in black, electron flow lines plotted in white, and $B_z - B_0$ plotted as the background color. Subtracting the initial guide field from B_z reveals the quadrupole signature in the out of plane magnetic field component, which is seen in two-fluid Hall MHD simulations,[27–29]. Although due to the asymmetry of the X-point flows the signature does not have a regular quadrupolar shape. The quadrupolar signature arises from the circular motion of electron currents in the region, as they decouple from the ion flow, that enhances the out-of-plane magnetic field. Anticlockwise electron motion will create a negative enhancement in the magnetic field, as can be seen in the top-left and bottom-right of Fig. 5, whereas clockwise electron motion creates a positive enhancement, as at top-right and bottom-left.

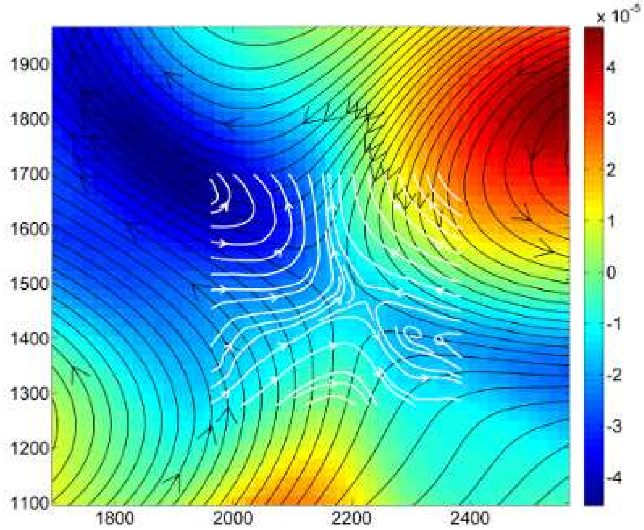

FIG. 5. Out of plane magnetic field component ($B_z - B_0$) showing quadrupolar signature around reconnection site 2.

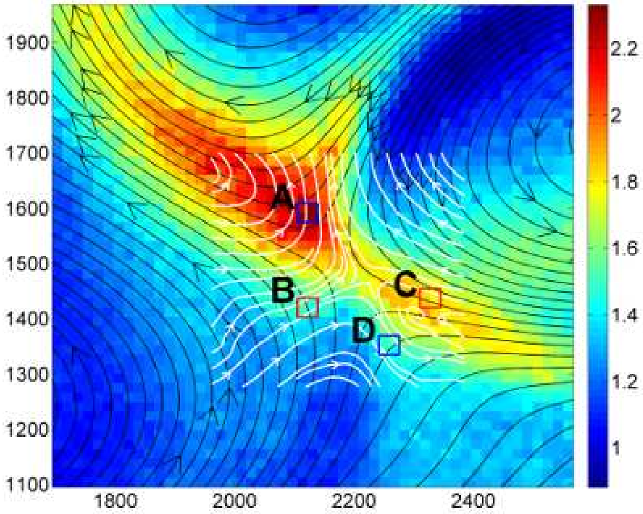

FIG. 6. Electron temperature anisotropy ratio $T_{e\|}/T_{e\perp}$ around reconnection site 2. Magnetic field lines are shown in black and electron bulk drifts are shown in white. The four marked regions are discussed in the text.

Figure 6 shows the distinctive shape of the region of increased electron temperature anisotropy generated around reconnection site 2. Two main areas of strong temperature anisotropy are located to the top-left and the bottom-right of the center of reconnection. An animation of the anisotropy, starting from an earlier time-step, shows that the anisotropy emerges from the center of reconnection (see supplementary material 7), and that the anisotropy increases as the reconnection rate increases. Four small boxes, labeled A, B, C and D are also shown in Fig. 6, corresponding to locations of electron in-flow (B and C) and electron out-flow (A and D). Later we will discuss the electron velocity space distribution functions (VDF) seen in these regions.

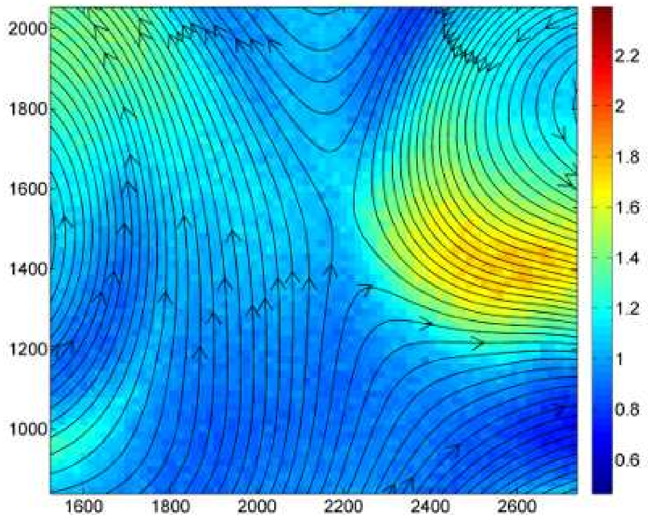

FIG. 7. Video of electron parallel temperature anisotropy generation $T_{e\|}/T_{e\perp}$ in the region of reconnection site 2 (enhanced online).

B. Reconnection Rate and Temperature

In the 2-D simulation geometry the rate of reconnected flux, i.e., the reconnection rate, is equal to the out of plane electric field E_z. This can be demonstrated as follows: The electric field is given by

$$\mathbf{E} = -\nabla V - \frac{\partial \mathbf{A}}{\partial t}, \tag{1}$$

where **A** is the magnetic vector potential and V is the electrostatic potential. Since the field lines in 2-D can be represented by contours of constant A_z, the rate of in-plane reconnection depends only on A_z. Given the two-dimensionality of the simulation, with z as the ignorable coordinate, it follows that Eq. 1 can be reduced to:

$$E_z = -\frac{\partial A_z}{\partial t}, \tag{2}$$

which confirms that E_z will give the reconnection rate at the center of any identified reconnection site.

For the identified reconnection events their centers were tracked during their motion in the course of the simulation and E_z recorded, as were parameters such as electron temperature and anisotropy, averaged over a box size of 15 square cells centered on the reconnection site. Measured reconnection rates were consistent with the animations of magnetic field line motion, further evidence that reconnection was occurring. Figure 8 shows time series for the resulting data from reconnection site 2. The top panel shows reconnection rate, the middle panel shows average electron temperature and the lower panel shows average electron anisotropy in terms of the parameter $(1 - T_{e\|}/T_{e\perp})$. In this figure an anisotropy parameter value less than zero corresponds to a parallel temperature anisotropy.

As previously noted, the electron temperature is not distinctly greater around reconnection sites when compared with

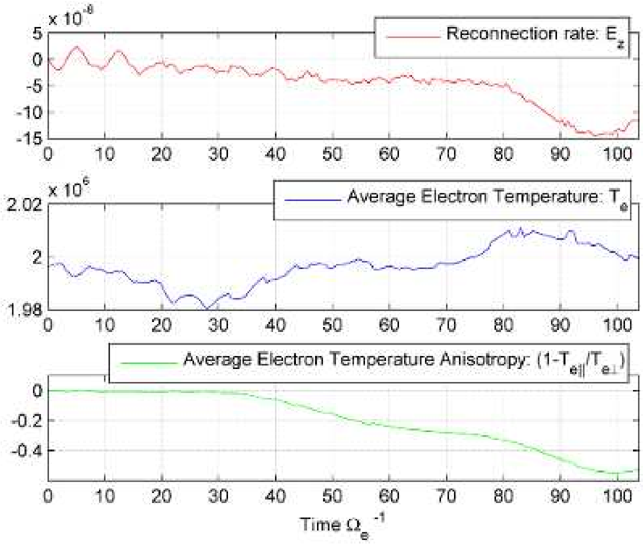

FIG. 8. Reconnection rate, electron temperature and temperature anisotropy parameter averaged around reconnection site 2 as a function of time.

other temperature variations in the simulation. Comparing the time profiles of Fig. 8, there is not an obvious correlation between electron temperature and reconnection rate around reconnection site 2. However, a correlation is evident between electron temperature anisotropy and reconnection rate E_z, indicating that the reconnection process is responsible for the anisotropy. As previously stated not all reconnection sites show such a marked increase in anisotropy, which suggests a more complex physical process is operating rather than a simple, local one which produces an absolute correlation with reconnection rate.

Animations show that electron temperature fluctuations across the simulation are dynamic, showing strong inhomogeneity between neighboring islands and temporal variability at X-point regions. With the use of a realistic electron-proton mass ratio, the high mobility of any locally energized electrons quickly leads to spatial inhomogeneity of electron temperature, which could explain why the temperature at reconnection regions is not significantly larger than at other points. There are also electron temperature changes which are clearly not associated with X-point reconnection at other locations within the simulation box. For example, within magnetic islands the electron temperature changes as the particle distribution evolves by compression or expansion, as in the suggestion that electrons can be accelerated in magnetic islands (formed in a reconnection layer) as they contract.[30]

C. Electron velocity distribution functions

We now discuss the velocity distributions seen near the reconnection site shown in Fig. 6. Four sub-regions are chosen on different sides of the magnetic separatrices corresponding to locations of electron in-flow (B and C) and electron outflow (A and D). Figure 9 shows the form of the electron distribution in the region of inflow box A, where the anisotropy is highest. Figure 9(a) shows the distribution in the $v_y - v_x$ plane, with the black cross showing the electron bulk drift; Fig. 9(b) shows the distribution in the $v_z - v_x$ plane, with the black arrow indicating the direction of the magnetic field; and Fig. 9(c) shows the distribution in the $v_\perp$ - $v_\|$ plane. All distributions are normalized to unity with red contours indicating higher particle density than blue. Velocity is normalized to the speed of light.

From Fig. 9(c) it can be seen that thermal width of the distribution in the parallel direction is approximately 1.5 times that in the perpendicular direction, in agreement with the anisotropy ratio of approximately 2.3 shown in Fig. 6. Rather than a bi-Maxwellian shape, the distribution shows a double peaked, beam-like structure, with one peak on the anti-parallel side and another peak on the parallel side of the distribution. The drift velocity in the positive y direction is consistent with the flow pattern of Fig. 6. The symmetry of the v_z - v_x distribution around the magnetic field direction seen in Fig. 9(b) shows that the electron distributions are approximately gyrotropic.

Figure 10 shows plots of the $v_\perp$ - $v_\|$ distribution functions for the other three boxes B, C, and D marked in Fig. 6. These all show multi-peaked structures. For example, Fig. 10(c) box D has the appearance of a core plus beam distribution, as the peak on the parallel side of the distribution is much larger. The distribution for box C in Fig. 10(b) even shows a triple peaked distribution. Thus the regions of largest temperature anisotropy in Fig. 3, which occur around reconnection sites, seem to correspond to the presence of distribution functions with a mix of multiple peaks. This, in itself, suggests that the reconnection process is forming one or both of these peaks, possibly by accelerating a subset of particles to form a second peak.

D. Particle Tracking

In order to determine the source of these multi-peaked distributions, we track particle trajectories of electrons selected from the peaks of the distributions, to determine whence these separate populations of electrons originate. Although the complex physics cannot be understood merely in terms of single particle motions, this exercise will allow us to show whether one or both of the distribution function peaks have been produced by electrons being accelerated or decelerated as they approach and interact with the reconnection site.

We show data for two electrons whose positions were tracked throughout the simulation, and their velocities analyzed. Both electrons were chosen from the recorded particles that interacted with reconnection site 2, and belong to the collection of simulation particles in box A. Electron E1 (Figs. 11 and 12) was chosen from the particles in the peak on the parallel side of the distribution shown in Fig. 9(c). Electron E2 (Figs. 13 and 14) was chosen from the particles in the peak on the anti-parallel side of the distribution. In this figure time is shown in units of the electron cyclotron period calculated using magnetic field B_0. In Fig. 11, the upper panel shows

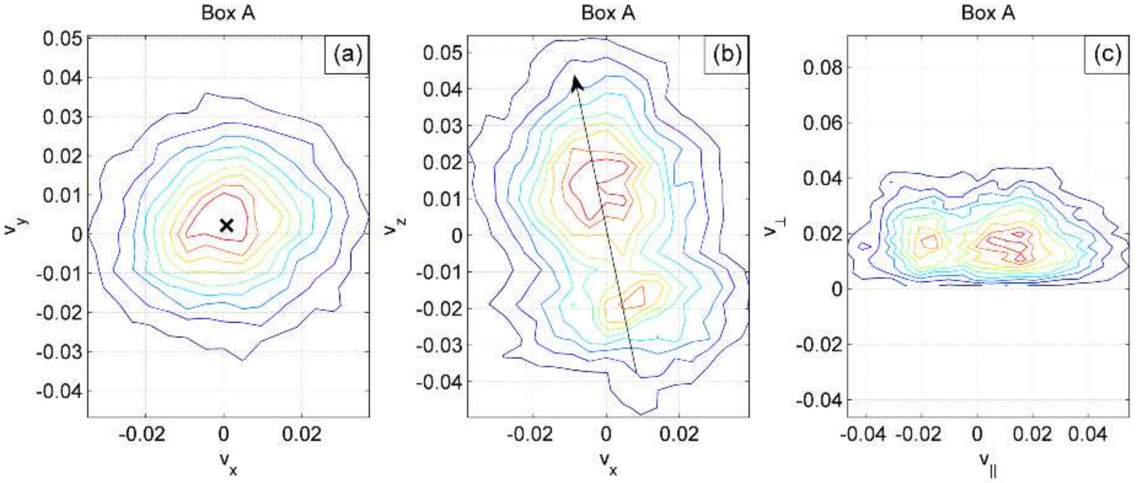

FIG. 9. Electron VDF for reconnection site 2, box A, as shown in Fig. 6.

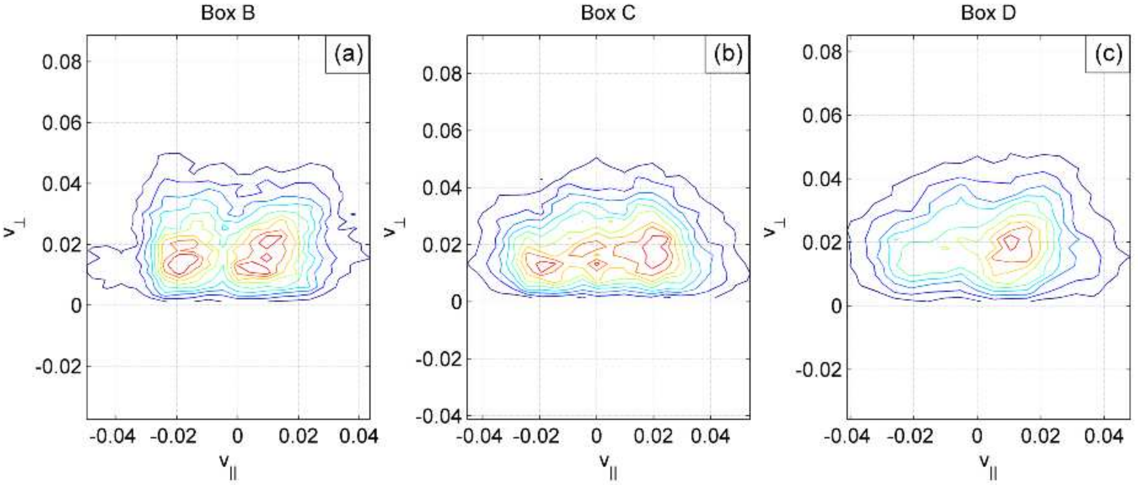

FIG. 10. Electron VDF for reconnection site 2, for (a) box B, (b) box C and (c) box D.

v_z versus time for electron E1. Velocity components v_x and v_y are shown in the next panel in blue and green, respectively. The electric field as seen by electron E1 is shown in the lower two panels, with E_x and E_y plotted in blue and green, and E_z in red. Figure 12 shows the trajectory taken by electron E1 up until and during its encounter with the reconnection site. Magnetic field line contours for the whole simulation box are shown in black. Traced in white are the electron position for the interval $T = 0$ to $T = 100\Omega_e^{-1}$. The green and blue crosses on the trajectory plots mark the start and end locations, respectively. The black cross marked on the red v_z and E_z time-series, corresponds to the time at which the magnetic field lines are shown, with a corresponding red cross marked on the electron trajectory plots at the same time step.

Figure 11 clearly shows that as electron E1 encounters the reconnection region after $T\Omega_e/2\pi = 9$ the parallel z component of its velocity increases. This is one example of many particles that were tracked, and all show similar behavior. Electrons experience an acceleration, due to E_z, along the guide field direction as they approach the reconnection site. The large increase in negative E_z in Fig. 11 results in a force on electron E1 in the positive z direction. Figure 8 shows that E_z for reconnection site 2 (i.e., at the center of the reconnection region) is mainly negative throughout the simulation. Figure 11 also indicates that electron E1 passes very close to the center of reconnection, since the oscillation in v_z decreases in amplitude, indicating that the in-plane components of the magnetic field have become almost zero. In summary, reconnection site 2 is responsible for the positive parallel peaks in Figs. 9 and 10.

We now turn to the behavior of electrons in the anti-parallel peak of the distribution function. Figures. 13 and 14 show trajectory information for electron number E2, which is from the peak on the anti-parallel side of the distribution of Fig. 9.

This particle has experienced acceleration in the negative

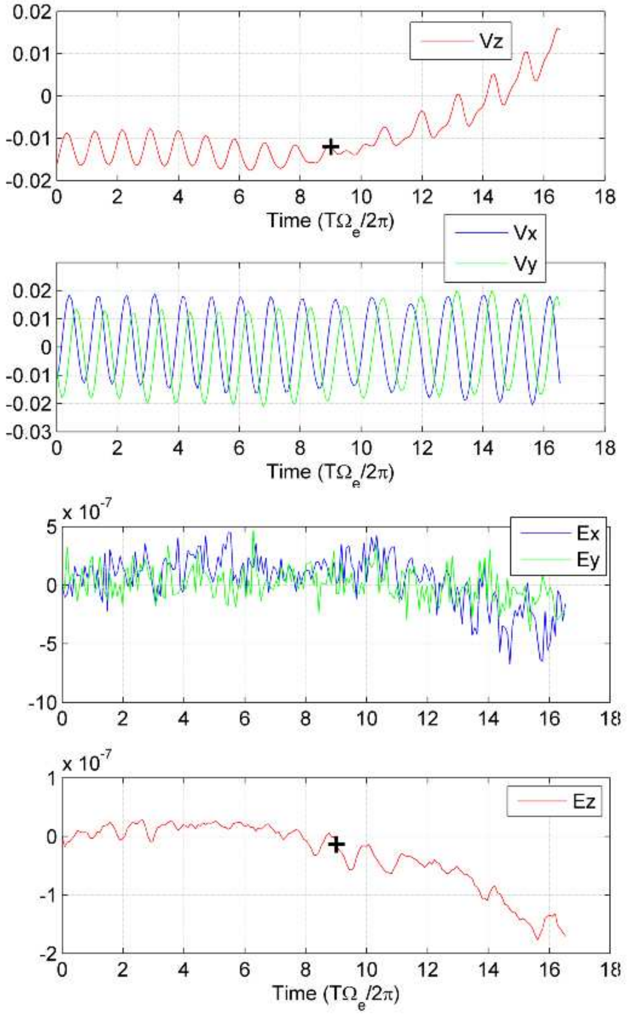

FIG. 11. Particle velocity and electric field (as seen by the particle) for electron E1 which interacts with reconnection site 2.

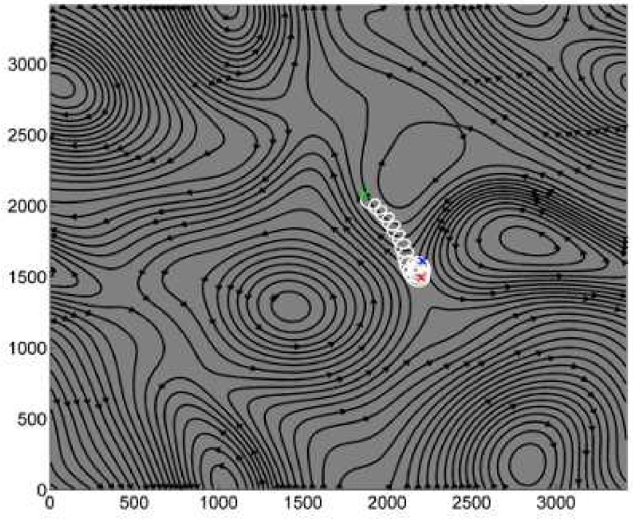

FIG. 12. Trajectory of electron E1 as it approaches and interacts with reconnection site 2. Magnetic field lines are shown in black at the time indicated by the black and red crosses in

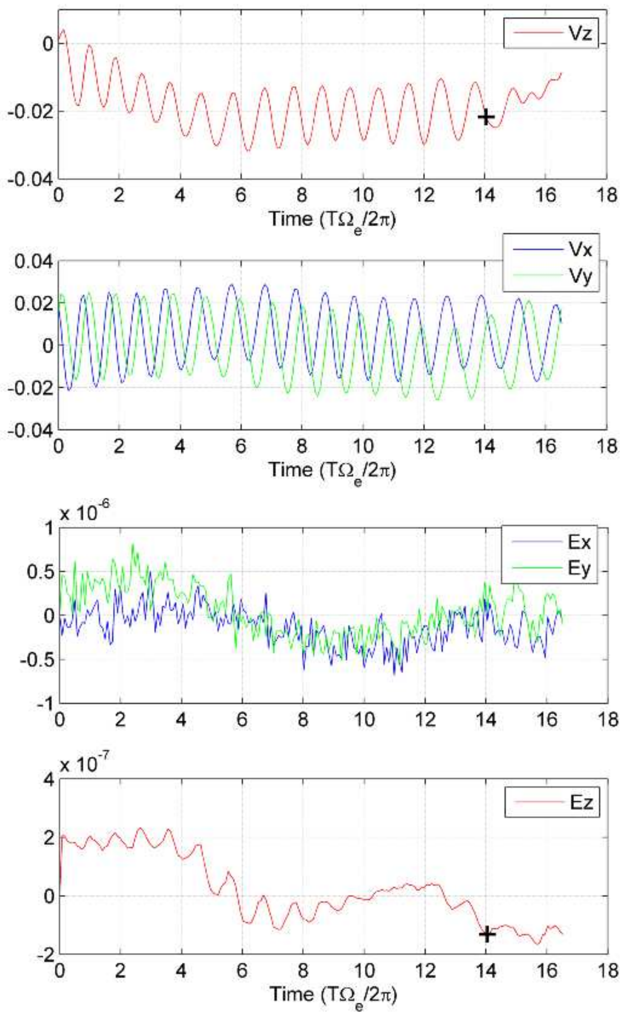

FIG. 13. Particle velocity and electric field (as seen by the particle) for electron E2 which interacts with reconnection site 2.

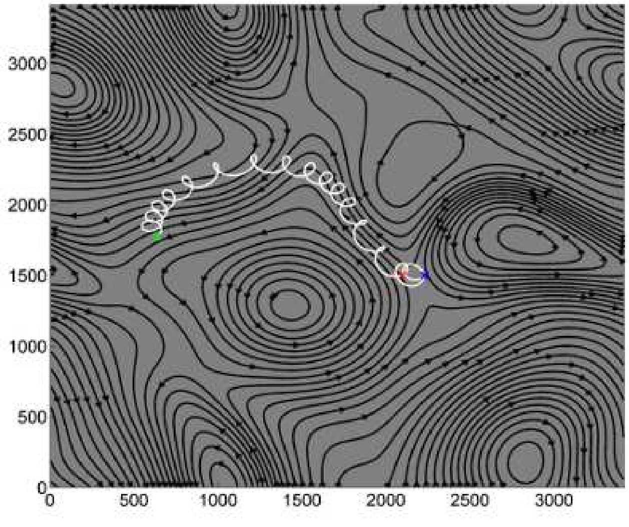

FIG. 14. Trajectory of electron E2 as it approaches and interacts with reconnection site 2. Magnetic field lines are shown in black at the time indicated by the black and red crosses in Fig. 13.

z direction before it encounters the reconnection site at approximately $T\Omega_e/2\pi = 14$. However, as it approaches the reconnection site it, like electron E1, experiences a positive acceleration, after it enters the reconnection region. This is consistent with the negative E_z associated with the sense of reconnection at this site. However, despite this acceleration the particle's v_z velocity remains negative. We have examined other particles from this peak and they show a similar history. From Figs. 12 and 14 electrons E1 and E2 have very different trajectory histories, but are eventually colocated but with separate parallel velocities.

Since reconnection site 2 mainly has negative E_z for most of the simulation, it accelerates electrons in the positive z direction. We have used this fact to confirm this mechanism of temperature anisotropy generation, by plotting the positions in previous time-steps of groups of particles from the negative peaks of Figs. 9 and 10. The trajectories of these particles traced a region whose shape was towards the center of reconnection only from the top left part of the separatrix and the bottom right part of the separatrix, consistent with the shape of the region of enhanced parallel anisotropies in these locations, as in Fig. 6.

In order to determine why a triple peaked distribution is formed, as shown in box C Fig. 10, particles from the central peak were also tracked. Although not shown here, these particles again show positive increases in v_z near the reconnection site. So the central peak is formed of particles that start with a negative v_z but as they enter the reconnection site they are only accelerated enough to finish in the center of the distribution. So double or triple peaked distributions can be formed by electrons passing through multiple acceleration regions, but which arrive at the same location within a reconnection site.

IV. CONCLUSIONS

We have presented the results of 2-D simulations with realistic mass ratio of the turbulent decay of large scale fluctuations with a guide field out of the simulation plane. As in previous similar work with the guide field in the simulation plane,[18] a power spectrum of fluctuations quickly develops which extends to small scales of order the electron gyroradius. The power spectrum has an approximately power law dependence with wavenumber until $k\rho_e = 1$, with a gradual steepening thereafter until the noise floor of the simulation is reached. With the guide field out of the simulation plane, and the initial fluctuations of sufficient amplitude, the initial field configuration contains a number of magnetic field line X-points and islands. During the course of the simulation the X-points develop dynamically, moving with the motion of surrounding islands as the turbulence evolves. Animations show that the topology of field lines can change as they move through the X-points, from closed within a single island to circulating around several islands. The sense and rate of field line motion can change direction at any one particular X-point as the islands surrounding it grow and shrink. During the course of the simulation a number of the initial X-points disappear, and this is most likely to happen after the scale of the X-point becomes less than the local electron gyrodiameter. Thus the simulation sees a relaxation of the initial magnetic topology, as well as a redistribution of power from large to short scales.

The regions around X-points have signatures which indicate that magnetic reconnection is occurring. The sense and rate of reconnection (i.e., the sign and magnitude of the out of plane electric field) can change at any one particular X-point during the course of the simulation. The motion of field lines and the pattern of electron bulk drifts is found to be consistent with reconnection inflows and outflows. The electron flow pattern is clearly seen despite the reconnection region being only of the scale of a few electron gyroradii. The magnetic field line geometry in the neighborhood of the reconnection site is dominated by its surrounding magnetic islands, so that the reconnection flow and field line patterns are often asymmetric. This leads to the centers of the flow and magnetic field patterns being offset from each other, sometimes by as much as 100 λ_D. Where there is a clear pattern of reconnection associated electron drifts we also observe a quadrupolar signature in B_z, similar to that found in Hall reconnection. This is not surprising given that the X-point scale is much less than ion inertial and gyro-scales, so that the electron and ion motion are decoupled. Generally there are similar asymmetries in the quadrupolar signature as in the flow pattern. Because of the relatively small size of the simulation (the largest scale is of order the ion inertial length), the initial number and shape of the islands, we do not see the formation of narrow (small aspect ratio) current layers with embedded X-points. A larger simulation, with initial fluctuation injection at larger scales, or with initial power anisotropy may produce a different geometry of initial X-points with narrow current sheets as seen in MHD simulations[17] and some PIC simulations.[19]

Examination of the electron temperature variations in the simulation shows that there are no obviously dominant "hot spots" unique to the locations of magnetic reconnection. The variations of temperature at locations away from X-points seems to be not strongly different from those seen around X-points. On the other hand, animations of plots of the electron temperature anisotropy ratio $T_{e\|}/T_{e\perp}$ indicate enhanced parallel anisotropy at some X-points, and the dynamic appearance of regions of enhanced parallel anisotropy in reconnection outflow regions during periods of strong reconnection. There is not a unique one-to-one correspondence between X-points and regions of enhanced anisotropy, but this behavior is seen frequently. We have shown that the enhanced anisotropy is due to multi-peaked velocity distribution functions. This is the first time (to our knowledge) that such velocity space structures have been reported at this scale and in turbulence. Further investigation reveals that such distributions are not unique to reconnection outflow regions, but can be found elsewhere in the simulation.

In order to determine how these velocity space features are formed, and if the reconnection sites are responsible, electrons from the peaks of the distribution were tracked through their simulation history. These show that electrons experience acceleration due to the reconnection electric field E_z in the direction of the guide field when they are close to the reconnection site center. The reconnection sites in the simulation can accelerate electrons in both positive and negative z directions depending on the sense of reconnection at a particular X-point. Particle tracking allows us to give an explanation of the mechanism of anisotropy generation: The main peak of the distribution is generated by the local reconnection site, with the direction being set by the sense of reconnection, i.e. the sign of E_z. The outflow of electrons with the shifted v_z distribution will then potentially mix with the surrounding population of electrons. Large anisotropies therefore form around a reconnection site whose outflow area already has a population of electrons shifted in v_z in the opposite sense to that of the local reconnection site. This produces the double peaked distributions which are seen. This mechanism explains why not all reconnection sites in the simulation show this large temperature anisotropy signature, it depends on both the current direction of reconnection for the site, and the presence of a population of electrons oppositely shifted in velocity in its outflow region. In this picture the reconnection sites act as mixing zones where electrons can be accelerated. It is also possible to explain in this scenario the presence of triple-peaked distribution functions which are sometimes seen.

The question of accessibility of any location to electrons with some given parallel velocity depends on the time history of both particles and field lines. The topological history of field lines passing through the reconnection X-point is thus crucial to the mixing of velocity space components. Electrons accelerated at, or near to, one X-point are close to field lines around the separatrices between islands, and therefore have possible connection to other X-points. On the other hand electrons on field lines deep within a magnetic island, which thus do not participate in reconnection, are likely to remain within that island. Of course, the fate of electrons in magnetic islands also depends indirectly on reconnection since it mediates the change of island field topology.

In summary, we have successfully identified reconnection sites in the simulation. We have found, even at these small scales, a fluid like configuration of electron bulk drifts through the reconnection sites. We also see the quadrupolar out of plane magnetic field signature of Hall reconnection, and consistent with the election flow pattern. Electron velocity distribution functions in these regions are multi-peaked, and particle tracking has shown that the reconnection sites are responsible for accelerating the electrons along the guide field. The reconnection direction (the sign of E_z) controls the direction of acceleration, and thus reconnection regions can generate large parallel anisotropies in specific regions around them, where the field line topology allows access by particles with opposite directed velocities.

The reconnection process not only provides a mechanism to transfer magnetic energy to kinetic energy but it also provides mixing sites within the turbulent plasma to allow the generation of multi-peaked velocity distribution functions, which can be the free energy source for the formation of waves. We expect the multi-peaked distributions to be unstable preferentially for parallel propagating waves, but given the guide field direction and 2-D nature of our simulation it is unlikely that the unstable waves are supported. In a full 3-D simulation we suggest that these multi-peaked distributions would form further waves via instabilities in the plasma. It is not clear what the full effect of this would be in terms of electron scattering or magnetic field line topology, given that in a 3-D simulation the reconnection sites themselves will have their own three dimensional dynamics. However, in future work we will consider what type of instabilities might associated with these distributions.

Our simulations have shown that reconnection is crucial to understanding the production of electron parallel temperature anisotropy in turbulence. This implies turbulence may play an active role in increasing electron parallel temperature anisotropy. However, recent work on the evolution of the solar wind has highlighted the importance of kinetic instabilities in limiting the particle temperature anisotropy in response to forcing from the expansion of the solar wind.[31,32] The applicability of the current work to solar wind turbulence can be questioned because of the scale and large amplitudes of the initial fluctuations used in the simulations. These have been adopted due to constraints of realistic mass ratio, and the requirement to resolve a turbulent cascade above the noise floor of the simulation. Thus the current work might be more applicable to large amplitude turbulence behind the quasi-parallel terrestrial bow shock[14] or in current sheets in the solar wind where some evidence of enhanced dissipation exists.[15] The anisotropy generation mechanism which we have described may be important in these situations to the cascade of energy to smaller scales within collisionless plasma turbulence.

Finally, we return to the question of dissipation in turbulence in a collisionless plasma. In our simulations reconnection is responsible for velocity space mixing and non-locality of velocity space components. Crucial for this behavior is the topological evolution of field lines passing through reconnection sites which allow long-range accessibility to distant locations and other reconnection sites. Electrons within islands have a different and more restricted accessibility. This has implications for the statistics of particles in the turbulence and the appropriate description of their behaviour. The power spectrum of fluctuations that we observe develops rapidly after the start of the simulation, and has a power law form which is relatively time-steady. It does not seem directly influenced by reconnection, the dynamic behavior of X-points or the evolution of the electron temperature anisotropy. Since the electron behavior is crucially dependent on the topological evolution of the magnetic field, it seems possible that dissipation at the smallest scales in a collisionless plasma might be most influenced by how topological complexity, rather than fluctuation power, is carried to small scales.

ACKNOWLEDGMENTS

CTH is supported by an STFC (UK) studentship, and DB by STFC grant ST/J001546/1.

REFERENCES

[1] V. Carbone, Space Science Reviews **172**, 343 (2012).

[2] J. W. Bieber, W. Wanner, and W. H. Matthaeus, J. Geophys. Res. **101**, 2511 (1996).

[3] R. T. Wicks, T. S. Horbury, C. H. K. Chen, and A. A. Schekochihin, MRNAS **407**, L31 (2010).

[4] L. Matteini, P. Hellinger, S. Landi, P. Trvnek, and M. Velli, Space Science Reviews **172**, 373 (2012).

[5] O. Alexandrova, V. Carbone, P. Veltri, and L. Sorriso-Valvo, The Astrophysical Journal **674**, 1153 (2008).

[6] F. Sahraoui, M. L. Goldstein, G. Belmont, P. Canu, and L. Rezeau, Phys. Rev. Lett. **105**, 131101 (2010).

[7] S. D. Bale, P. J. Kellogg, F. S. Mozer, T. S. Horbury, and H. Reme, Phys. Rev. Lett. **94**, 215002 (2005).

[8] O. Alexandrova, C. Lacombe, A. Mangeney, R. Grappin, and M. Maksimovic, The Astrophysical Journal **760**, 121 (2012).

[9] G. Paschmann, Geophys. Res. Lett. **35**, L19109 (2008).

[10] J. T. Gosling and A. Szabo, J. Geophys. Res. **113**, A10103 (2008).

[11] N. Katz, J. Egedal, W. Fox, A. Le, J. Bonde, and A. Vrublevskis, Phys. Rev. Lett. **104**, 255004 (2010).

[12] J. Birn, L. Fletcher, M. Hesse, and T. Neukirch, Astrophys. J. **695**, 1151 (2009).

[13] S. Servidio, P. Dmitruk, A. Greco, M. Wan, S. Donato, P. A. Cassak, M. A. Shay, V. Carbone, and W. H. Matthaeus, Nonlinear Processes in Geophysics **18**, 675 (2011).

[14] A. Retinò, D. Sundkvist, A. Vaivads, F. Mozer, M. André, and C. J. Owen, Nature Phys. **3**, 236 (2007).

[15] K. T. Osman, W. H. Matthaeus, A. Greco, and S. Servidio, Astrophys. J. Lett. **727**, L11 (2011).

[16] S. Bourouaine, O. Alexandrova, E. Marsch, and M. Maksimovic, The Astrophysical Journal **749**, 102 (2012).

[17] S. Servidio, W. H. Matthaeus, M. A. Shay, P. A. Cassak, and P. Dmitruk, Phys. Rev. Lett. **102** (2009), 10.1103/PhysRevLett.102.115003.

[18] E. Camporeale and D. Burgess, Astrophys. J. **730**, 114 (2011).

[19] H. Karimabadi, V. Roytershteyn, M. Wan, W. H. Matthaeus, W. Daughton, P. Wu, M. Shay, B. Loring, J. Borovsky, E. Leonardis, S. C. Chapman, and T. K. M. Nakamura, Physics of Plasmas **20**, 012303 (2013).

[20] G. G. Howes, W. Dorland, S. C. Cowley, G. W. Hammett, E. Quataert, A. A. Schekochihin, and T. Tatsuno, Phys. Rev. Lett. **100**, 065004 (2008).

[21] O. Chang, S. Peter Gary, and J. Wang, Geophys. Res. Lett. **38**, L22102 (2011).

[22] C. S. Salem, G. G. Howes, D. Sundkvist, S. D. Bale, C. C. Chaston, C. H. K. Chen, and F. S. Mozer, Astrophys. J. Lett. **745**, L9 (2012).

[23] D. Perrone, F. Valentini, S. Servidio, S. Dalena, and P. Veltri, The Astrophysical Journal **762**, 99 (2013).

[24] M. P. Leubner, Physics of Plasmas **11**, 1308 (2004).

[25] S. Markidis, E. Camporeale, D. Burgess, Rizwan-Uddin, and G. Lapenta, in *Numerical Modeling of Space Plasma Flows: ASTRONUM-2008*, Astronomical Society of the Pacific Conference Series, Vol. 406, edited by N. V. Pogorelov, E. Audit, P. Colella, and G. P. Zank (2009) p. 237.

[26] C. W. Smith, K. Hamilton, B. J. Vasquez, and R. J. Leamon, Astrophys. J. Lett. **645**, L85 (2006).

[27] B. Sonnerup, Vol. Ill,(LT Lanzerotti, CF Kennel, and EN Parker, eds.), North Holland , 45 (1979).

[28] T. Terasawa, Geophysical Research Letters **10**, 475 (1983).

[29] H. Karimabadi, J. D. Huba, D. KraussVarban, and N. Omidi, Geophysical Research Letters **31** (2004), 10.1029/2004GL019553.

[30] J. F. Drake, M. Swisdak, H. Che, and M. A. Shay, Nature **443**, 553 (2006).

[31] E. Camporeale and D. Burgess, Journal of Geophysical Research: Space Physics **113**, n/a (2

[32] Š. Štverák, P. Trávníček, M. Maksimovic, E. Marsch, A. N. Fazakerley, and E. E. Scime, Journal of Geophysical Research (Space Physics) **113**, A03103 (2008).